Journal of Solid State Chemistry 183 (2010) 2987–2994

Contents lists available at ScienceDirect

Journal of Solid State Chemistry

journal homepage: www.elsevier.com/locate/jssc

Structural relationships between new carbide $La_{14}Sn(MnC_6)_3$ and fully ordered $La_{11}(MnC_6)_3$

Julia V. Zaikina [a,*], Haidong Zhou [b], Susan E. Latturner [a,*]

[a] Department of Chemistry and Biochemistry, Florida State University, 95 Chieftan Way, Tallahassee, FL 32306, USA
[b] National High Magnetic Field Laboratory, Florida State University, Tallahassee, FL 32306, USA

ARTICLE INFO

Article history:
Received 11 August 2010
Received in revised form
29 September 2010
Accepted 3 October 2010
Available online 13 October 2010

Keywords:
La/Ni eutectic
Ternary carbides
Superstructure
Flux synthesis
Intermetallic
Manganese

ABSTRACT

Crystals of the ternary $La_{11}(MnC_6)_3$ and new quaternary carbide $La_{14}Sn(MnC_6)_3$ phases were grown from La/Ni eutectic flux and their structures were determined by means of X-ray single crystal diffraction. $La_{11}(MnC_6)_3$ is a new superstructure variant of $La_{3.67}MnC_6$ (previously reported disordered subcell: $P6_3/m$; $a_0=8.806$ Å; $c_0=5.329$ Å, $Z=2$). The superstructure ($R\bar{3}$; $a=\sqrt{3}a_0=15.2649(9)$ Å; $c=3c_0=16.013(1)$ Å, $Z=6$; $R_1=0.022$) is realized by complete ordering of the La chains within the columns of face-sharing carbon octahedra, with alternating La–La distances leading to *R*-centering and enlargement of the unit cell. The structure of the quaternary carbide $La_{14}Sn(MnC_6)_3$ ($P\bar{6}$; $a=8.756(1)$ Å; $c=10.483(2)$ Å, $Z=1$; $R_1=0.026$) is closely related to that of $La_{11}(MnC_6)_3$ with part of the MnC_6 units replaced by Sn atoms. The structure and precise composition of $La_{14}Sn(MnC_6)_3$ can be derived from that of $La_{11}(MnC_6)_3$ by taking into account the extent of this substitution and variation in lanthanum siting in the chain of carbon octahedra. Band structure calculations indicate both phases are metallic; the $La_{11}(MnC_6)_3$ phase is stabilized by the ordering of La atoms which induces a pseudogap at E_F.

1. Introduction

The ternary carbides of rare-earth (*RE*) and transition (*T*) metals $RE_xT_yC_z$ are being extensively investigated owing to their diverse crystal structures and physical properties such as hardness, magnetism, and superconductivity [1]. They are also of interest from a theoretical point of view [2]. Metal carbide compounds can be divided into two groups according to the metal-to-carbon ratio, $(x+y)/z$. Carbides with low carbon content called carbometallates have isolated C^{4-} specimens, while carbides with high carbon content feature carbon pairs C_2 and more rarely linear C_3 units [3].

The family of isostructural carbides $RE_{3.67}TC_6$ (*RE*=La–Nd, Sm; *T*=Fe, Ru, Mn) was first reported by Witte and Jeitschko in 1996 [4]. These phases crystallize in the hexagonal space group $P6_3/m$ and feature trigonal planar $T(C_2)_3$ groups with the transition metal coordinated to one of the carbon atoms of the C_2 units. The short C–C distance in these units indicates the presence of a double bond. In the structure of $La_{3.67}FeC_6$ electropositive La atoms form a framework around the $Fe(C_2)_3$ anions; additional La atoms are found within a column of face-sharing carbon octahedra formed by the terminal carbon atoms of the C_2 units. The La site within this column is partially occupied, to allow for optimized La–La distances longer than 3.40 Å. Recently, the structure of $La_{3.67}FeC_6$ was reinvestigated and a superstructure (still in space group $P6_3/m$) with a tripled *c*-axis and partial ordering of the La atoms within the chain was reported [5]. A similar kind of ordering was found for $La_{3.65}RuC_6$, which was refined as a commensurate modulated structure [6]. The compound studied in our work, $La_{11}(MnC_6)_3$, crystallizes with a new and completely ordered variant of the $RE_{3.67}TC_6$ structure.

The $RE_{3.67}TC_6$ phases are typically prepared by the traditional method of rare-earth-transition-metal carbide synthesis—arc-melting of the starting components followed by long-term annealing. However, several carbides can be also accessed by flux synthesis; the fluxes used are molten metals capable of dissolving carbon, such as lithium or sodium [7]. The recently introduced crystal growth from La/Ni eutectic flux [8] is an efficacious synthesis technique leading to the formation of complex intermetallics containing carbon, boron, and transition metals such as Fe, Mn, and Ru [8,9]. Here we report on synthesis of ternary $La_{11}(MnC_6)_3$ and new quaternary carbide $La_{14}Sn(MnC_6)_3$ from La/Ni eutectic. These two compounds exhibit a close structural relationship which is investigated by means of X-ray single-crystal and powder diffraction methods. The formation of the completely ordered superstructure of $La_{11}(MnC_6)_3$ may be facilitated by crystallization in metal flux.

2. Materials and methods

2.1. Preparation

The synthesis method used in this work is analogous to the previously described crystal growth of $La_{21}Fe_8Sn_7C_{12}$ from La/Ni eutectic flux [8]. The starting materials were stored and handled in

* Corresponding authors: Fax. +850 644 8281.
E-mail addresses: yzaikina@chem.fsu.edu (J.V. Zaikina), latturner@chem.fsu.edu (S.E. Latturner).

0022-4596/$ - see front matter © 2010 Elsevier Inc. All rights reserved.
doi:10.1016/j.jssc.2010.10.004

an argon-filled glove-box. Powders of lanthanum (99.9%, Alfa Aesar), manganese (Alfa Aesar, 99.6%), carbon (95–97%, Strem Chemicals), tin (99.9%, Fisher Chemicals), bismuth (99.9%, Strem Chemicals), antimony (99.5%, Strem Chemicals), and ingots of La–Ni eutectic (88:12 wt %, Alfa Aesar 99.9%) were used as-received. The reactant ratios used are: La:Mn:*M*:C=2.1:0.8:0.7:1.2 mmol (*M*=Sn,Bi,Sb) and La:Mn:C=1.1:0.3:1.8 mmol (total masses 0.43 g and 0.20 g, respectively). These reactants were sandwiched between layers of La/Ni eutectic (~1.4 g) in an alumina crucible (ID 6 mm), with a second alumina crucible filled with Fiberfrax and inverted above the reaction crucible to act as a filter during centrifugation. The alumina crucibles were placed into a silica tube, which was fused under vacuum of 10^{-2} Torr; the ampoule was then heated to 950 °C in 3 h, held at this temperature for 12 h, and then cooled to 850 °C in 10 h. The reaction mixtures were subsequently annealed for 48 h at 850 °C and then cooled to 600 °C in 84 h. At 600 °C the ampoule was removed from the furnace, quickly inverted, and placed into a centrifuge to decant the molten flux. To separate the crystals from residual La—Ni coating, samples were briefly left in air to preferentially oxidize the La-rich eutectic flux. Crystals were kept in argon-filled glove-box or in a refrigerator under paratone oil to prevent any further oxidation.

2.2. Elemental analysis

Semiquantitative elemental analysis was performed with energy-dispersive X-ray spectroscopy (EDXS) on a JEOL 5900 scanning electron microscope equipped with PGT Prism energy dispersion spectroscopy software. Crystals were oriented with a flat face perpendicular to the beam and analyzed using a 30 kV accelerating voltage and an accumulation time of 60 s. The carbon content was not determined due to the limitation of EDXS with light elements. The samples were also monitored for Ni and Al contamination, which may stem from the flux or be leached from the crucible, respectively. No Ni or Al was detected for the both $La_{11}(MnC_6)_3$ and $La_{14}SnMn_3C_{18}$ phases. In addition, no Sb or Bi was found in the crystals of $La_{11}(MnC_6)_3$ selected from the samples with starting compositions $La_{21}Mn_8Sb_7C_{12}$ or $La_{21}Mn_8Bi_7C_{12}$. The La/Sn ratio in $La_{14}SnMn_3C_{18}$ was found to be 14:1.

2.3. X-ray single-crystal structure determination

A crystal of $La_{11}(MnC_6)_3$ was selected from the sample with starting composition La:Mn:C=11:3:18 in 1.4 g of La/Ni eutectic, while the crystals of $La_{14}Sn(MnC_6)_3$ were found in the reaction with starting composition La:Mn:Sn:C=21:8:7:12 in 1.4 g of La/Ni eutectic. Crystals were mounted on glass fibers using epoxy. X-ray diffraction data were collected at room temperature for $La_{11}(MnC_6)_3$ and $La_{14}Sn(MnC_6)_3$, and at 150 K for a second crystal of $La_{14}Sn(MnC_6)_3$ on a Bruker SMART APEX2 CCD diffractometer equipped with a Mo$K\alpha$ X-ray tube (λ=0.71073 Å). The detector was placed at a distance of 6 cm from the crystal. Frames were collected with a ω-scan with width of 0.3°. The frames were integrated with the Bruker SAINT software package [10] using a narrow-frame integration algorithm to a maximum 2θ angle of 55–70°. Data sets were corrected for absorption effects using the empirical method (SADABS [11]). The structures were solved by direct methods and refined by a combination of least-squares refinement and difference Fourier maps on $|F^2|$ using the SHELX-97 software package [12].

In the case of $La_{11}(MnC_6)_3$ the data set was indexed in the *R*-centered trigonal unit cell with parameters a=15.2649(9) Å and c=16.013(1) Å. No additional systematic extinctions, except those corresponding to the *R*-lattice [*hkl*], $-h+k+l=3n$, were observed. Superstructure reflections of general *hkil*-type, which contradict the symmetry of the previously reported subcell ($P6_3/m$; a=8.8035 Å; c=5.3346 Å), have lower intensity ($I/I_0 \le 12\%$) compared to the reflections which can be indexed in subcell. The centrosymmetric space group $R\bar{3}$ (No 148) was chosen for the structure solution (R_{int}=0.031). During the refinement all positions were found to be fully occupied by one type of atom. The final refinement using anisotropic displacement parameters for all atoms led to the composition $La_{11}(MnC_6)_3$ with R_1=0.022.

The structure of $La_{14}Sn(MnC_6)_3$ was solved in the $P\bar{6}$ space group (No 174) (R_{int}=0.032). During the crystal structure refinement one of the La positions was found to be split into two sites, La(3) and La(3a) with 0.89(3)/0.11 ratio and distance of 0.31(2) Å between them. The atomic displacement parameters (ADP) were constrained to be equal for La(3) and La(3a) and refined anisotropically. The final refinement using anisotropic displacement for all atoms led to the composition $La_{14.00(6)}SnMn_3C_{18}$ with R_1=0.026. The refinement with the split positions, La(3) and La(3a), performed using the data collected at 150 K for a second crystal of $La_{14}Sn(MnC_6)_3$ selected from the same sample (Table S1–S3) reveals a similar (within 3 e.s.d.) ratio of La(3)/La(3a), 0.83(4)/0.17, thus confirming the proposed split-model.

The structure solutions were checked with the program Platon [13] and no additional symmetry was found. The details of the data collection and refinement are summarized in Table 1, the atomic parameters are given in Table 2, and selected interatomic distances are listed in Table 3.

2.4. X-ray powder diffraction

Crystals of $La_{11}(MnC_6)_3$ were selected from the sample with starting composition La:Mn:C=11:3:18; after scraping off any residual flux, the crystals were ground using an agate mortar in an argon-filled glove-box. The powdered sample was sealed in plastic tape. Data were collected on an original setup based on a Huber imaging plate Guinier camera 670 using Cu$K\alpha_1$ radiation (λ=1.54060 Å) with Ge crystal monochromator. X-ray patterns were acquired at 0.005° resolution at ambient temperature. During the data collection the sample was placed in a vacuumed sample space to prevent oxidation.

Table 1
Data collection and structure refinement parameters for $La_{11}(MnC_6)_3$ and $La_{14}Sn(MnC_6)_3$.[a]

Composition	$La_{11}(MnC_6)_3$	$La_{14}Sn(MnC_6)_3$
Space group	$R\bar{3}$ (No 146)	$P\bar{6}$ (No 174)
Collection temperature, K	295	
Cell parameters, *a*, Å	15.2649(9)	8.756(1)
***c*, Å**	16.013(1)	10.483(2)
***V*, Å^3**	3231.4(3)	696.0(2)
Z	6	1
Density (calc.), g cm^{-3}	5.89	5.83
μ, mm^{-1}	22.96	23.13
Data collection range, deg.	2 to 27.5	2 to 35
Absorption type	numerical	multi-scan
Reflections collected	11698	6856
Independent reflections	1641 [R_{int}=0.031]	1943 [R_{int}=0.031]
Parameters refined	98	66
R_1[b]	0.020	0.026
wR_2 [c] [$F_o > 4\sigma F_o$]	0.047	0.051
R_1, wR_2 (all data)	0.022, 0.047	0.026, 0.052
Largest diff. peak and hole, e/Å^3	1.009 and −1.167	2.464 and −1.519
Goodness-of-fit	1.341	1.138

[a] Further details of the crystal structure determination may be obtained from Fachinformationszentrum Karlsruhe, D-76344 Eggenstein-Leopoldshafen, Germany, on quoting the depository numbers CSD-422022 and CSD-422023 for $La_{11}(MnC_6)_3$ and $La_{14}Sn(MnC_6)_3$.

[b] $R_1=\sum||F_o|-|F_c||/\sum|F_o|$.

[c] $wR_2=[\sum w(F_o^2-F_c^2)^2/\Sigma w(F_o^2)^2]^{1/2}$, $w=[\Sigma^2(F_o^2)+(Ap)^2+Bp]^{-1}$; $p=(F_o^2+2F_c^2)/3$; A=0.0114 and B=37.6804 for $La_{11}(MnC_6)_3$; A=0.0070 and B=6.9628 for $La_{14}Sn(MnC_6)_3$.

Table 2
Atomic coordinates and equivalent displacement parameters for $La_{11}(MnC_6)_3$ and $La_{14}Sn(MnC_6)_3$.

Atom	Wyckoff	s.o.f.	x/a	y/b	z/c	U_{eq}[a]
$La_{11}(MnC_6)_3$						
La(1)	18*f*	1	0.15241(2)	0.24569(2)	0.08055(2)	0.00793(9)
La(2)	18*f*	1	0.15769(2)	0.24382(2)	0.41922(2)	0.00867(9)
La(3)	18*f*	1	0.24245(2)	0.09037(2)	0.24906(2)	0.00706(9)
La(4)	6*c*	1	0	0	0.13663(3)	0.0090(1)
La(5)	6*c*	1	0	0	0.36122(3)	0.0099(1)
Mn	18*f*	1	0.34178(5)	0.00454(5)	0.08374(5)	0.0079(2)
C(1)	18*f*	1	0.1330(4)	0.4205(3)	0.0820(3)	0.0078(9)
C(2)	18*f*	1	0.1896(4)	0.2378(4)	0.2489(3)	0.0075(9)
C(3)	18*f*	1	0.2517(3)	0.0501(3)	0.0841(3)	0.0083(9)
C(4)	18*f*	1	0.0930(4)	0.1596(4)	0.2488(3)	0.0092(9)
C(5)	18*f*	1	0.1879(4)	0.0867(4)	0.4149(3)	0.012(1)
C(6)	18*f*	1	0.1869(4)	0.0849(4)	0.0843(3)	0.011(1)
$La_{14.00(6)}Sn(MnC_6)_3$						
La(1)	6*l*	1	0.01158(5)	0.26378(4)	0.25500(3)	0.00944(7)
La(2)	3*j*	1	0.33516(6)	0.39510(7)	0	0.00797(9)
La(3)	3*k*	0.89(3)	0.3974(5)	0.4059(4)	$\frac{1}{2}$	0.0120(5)
La(3a)	3*k*	0.11	0.421(3)	0.388(2)	$\frac{1}{2}$	0.0120
La(4)	2*i*	1	$\frac{2}{3}$	$\frac{1}{3}$	0.17070(6)	0.0105(1)
Sn	1*b*	1	0	0	$\frac{1}{2}$	0.0143(2)
Mn(1)	2*h*	1	$\frac{1}{3}$	$\frac{2}{3}$	0.2623(2)	0.0078(3)
Mn(2)	1*a*	1	0	0	0	0.0083(4)
C(1)	6*l*	1	0.3744(8)	0.4810(8)	0.2555(5)	0.006(1)
C(2)	6*l*	1	0.381(1)	0.332(1)	0.2495(6)	0.015(1)
C(3)	3*j*	1	0.231(1)	0.043(1)	0	0.010(2)
C(4)	3*j*	1	0.404(1)	0.105(1)	0	0.011(2)

[a] U_{eq} is defined as one third of the trace of the orthogonalized U_{ij} tensor.

Table 3
Selected interatomic distances (Å) in the structures of $La_{11}(MnC_6)_3$ and $La_{14}Sn(MnC_6)_3$.

Distance, Å	$La_{11}(MnC_6)_3$	Distance, Å	$La_{14}Sn(MnC_6)_3$
La(1)–La(4)	3.3999(4)	La(1)–La(4) × 3	3.4801(6)
La(2)–La(5)	3.3986(4)	La(2)–La(4) × 3	3.6727(6)
La(3)–La(1)	3.6588(4)	La(4)–La(4)	3.578(1)
La(4)–La(5)	3.5963(7)	*La(3)–La(3a)*	*0.31(2)*[a]
La(4)–La(4)	4.3757(7)	Sn–La(1) × 5	3.4220(5)
La(5)–La(5)	4.4445(7)	Sn–La(3) × 4	3.4220(5)
Mn–C(1)	1.832(5)	Sn–La(3a) × 4	3.56(1)
Mn–C(2)	1.823(5)	Mn(1)–C(1) × 3	1.833(5)
Mn–C(3)	1.825(5)	Mn(2)–C(3) × 3	1.862(8)
Mn–La × 9	3.2016(7) – 3.6441(8)	Mn(1)–La(1) × 3	3.2323(5)
C(1)–C(5)	1.315(7)	Mn(1)–La(3) × 3	3.613(3)
C(2)–C(4)	1.357(7)	Mn(1)–La(3a) × 3	3.85(2)
C(3)–C(6)	1.337(7)	Mn(1)–La(2) × 3	3.640(1)
C(1)–La × 4	2.724(5) – 2.835(5)	Mn(2)–La(2) × 3	3.2294(6)
C(2)–La × 4	2.770(5) – 2.938(5)	Mn(2)–La(1) × 6	3.5005(5)
C(3)–La × 4	2.730(5) – 2.816(5)	C(1)–C(2)	1.337(9)
C(4)–La × 6	2.743(5) – 2.967(5)	C(3)–C(4)	1.33(1)
C(5)–La × 4	2.631(5) – 2.791(5)	C(1)–La × 4	2.679(6) – 2.845(6)
C(6)–La × 4	2.613(5) – 2.770(5)	C(2)–La × 4	2.630(8) – 2.983(7)
		C(3)–La × 4	2.738(2) – 2.870(8)
		C(4)–La × 5	2.768(8) – 2.932(4)

[a] The distance between two split sites.

The indexing of the X-ray powder pattern and refinement of the unit cell parameters was done using least-squares fitting employed in the WinCSD software package [14].

2.5. Differential scanning calorimetry (DSC) and thermogravimetric analysis (TGA)

To investigate the possible order–disorder phase transitions of $La_{11}(MnC_6)_3$, simultaneous DSC–TGA analysis was performed using a TA Instruments Q600 system under a flow of argon. In an open alumina pan, the powdered sample was heated to 1000 °C at a rate of 5 °C/min and cooled down to room temperature with the same rate.

2.6. Quantum-chemical calculations

Calculations of density of states (DOS) were performed with the tight binding-linear muffin tin orbitals-atomic sphere approximation TB-LMTO-ASA program package [15a], based on the experimentally determined room temperature unit cell dimensions and atomic coordinates for $La_{11}(MnC_6)_3$ and $La_{14}Sn(MnC_6)_3$. The radial scalar-relativistic Dirac equation was solved to obtain the partial waves. Interstitial empty spheres ($0.99\ Å \le r(E) \le 2.14\ Å$) were added to fill the interstitial space. The calculation was made for 40 ($La_{11}(MnC_6)_3$) and 250 ($La_{14}Sn(MnC_6)_3$) κ points in the irreducible Brillouin zone (IBZ). Integration over the Brillouin zone was made by the tetrahedron method [15b]. The following radii of atomic spheres were applied for the calculations: $La_{11}(MnC_6)_3$, $r(La(1))=3.63$ Å, $r(La(2))=3.58$ Å, $r(La(3))=3.84$ Å, $r(La(4))=3.50$ Å, $r(La(5))=3.54$ Å, $r(Mn)=2.46$ Å, $r(C(1))=1.51$ Å, $r(C(2))=1.52$ Å, $r(C(3))=1.49$ Å, $r(C(4))=1.52$ Å, $r(C(5))=1.51$ Å, $r(C(6))=1.49$ Å; $La_{14}Sn(MnC_6)_3$, $r(La(1))=3.61$ Å, $r(La(2))=4.00$ Å, $r(La(2))=3.80$ Å, $r(La(4))=3.92$ Å, $r(Sn)=3.87$ Å, $r(Mn(1))=2.55$ Å, $r(Mn(2))=2.61$ Å, $r(C(1))=r(C(2))=r(C(3))=r(C(4))=1.47$ Å. The basis sets contained La (6*s*, 5*d*, 4*f*), Mn (4*s*, 4*p*, 3*d*), Sn (5*s*, 5*p*) and C (2*s*, 2*p*) with La(6*p*), Sn (5*d*, 4*f*) and C(3*d*) functions being downfolded.

3. Results and discussion

3.1. Preparation

Crystals of $La_{11}(MnC_6)_3$ were initially found as a byproduct in reactions intended to produce $La_{21}Mn_8M_7C_{12}$ [16] (M=Sb or Bi) from La/Ni eutectic flux. Later syntheses of $La_{11}(MnC_6)_3$ were carried out in La/Ni flux with optimized starting composition

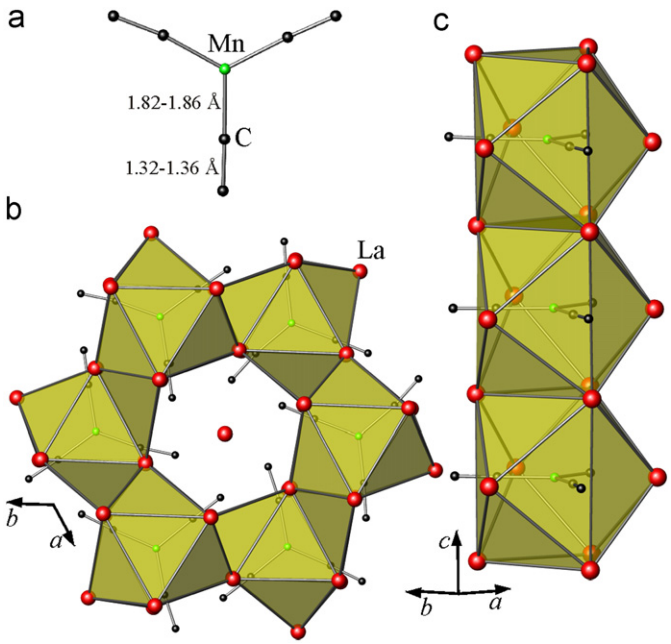

Fig. 1. (*a*) The trigonal planar unit $Mn(C_2)_3$ found in the crystal structures of $La_{11}(MnC_6)_3$ and $La_{14}Sn(MnC_6)_3$. (*b*) Framework of face-sharing tricapped trigonal prisms of La atoms around $Mn(C_2)_3$, i.e. MnC_6@La_9, in *ab*-plane, showing hexagonal channels filled with La atoms. (*c*) Stacking of face-sharing MnC_6@La_9 polyhedra along the *c*-axis in the crystal structure of $La_{11}[MnC_6]_3$.

La:Mn:C=11:3:18, i.e. with the absence of "foreign" elements (Sb or Bi), and with a more suitable La/Mn/C ratio. This leads to a higher yield of ~20% of $La_{11}(MnC_6)_3$ and larger crystal size (up to 0.5 cm, see Figure S1); the crystal of $La_{11}(MnC_6)_3$ used for structure determination by X-ray diffraction was selected from these later reactions. Well-crystallized specimens of $La_{14}Sn(MnC_6)_3$ (including the crystal for X-ray single-crystal determination) were found together with the cubic phase $La_{21}Mn_8Sn_7C_{12}$ [16] as products of a reaction with the starting composition La:Mn:Sn:C=21:8:7:12 in excess La/Ni flux. Modifying the reaction to produce only $La_{14}Sn(MnC_6)_3$ was not possible due to the presence of all four elements in both $La_{14}Sn(MnC_6)_3$ and $La_{21}Mn_8Sn_7C_{12}$; changes in reaction ratio and heating profile did not prevent formation of the cubic phase. However, the crystal habits of these two phases are distinctly different, and the rod-like crystals of $La_{14}Sn(MnC_6)_3$ can easily be distinguished from the truncated octahedra of the cubic $La_{21}Mn_8Sn_7C_{12}$. $La_{11}(MnC_6)_3$ also crystallizes as hexagonal rods of silver grey color. The compounds are air-sensitive, but withstand overnight data collection at ambient temperature by being embedded into epoxy.

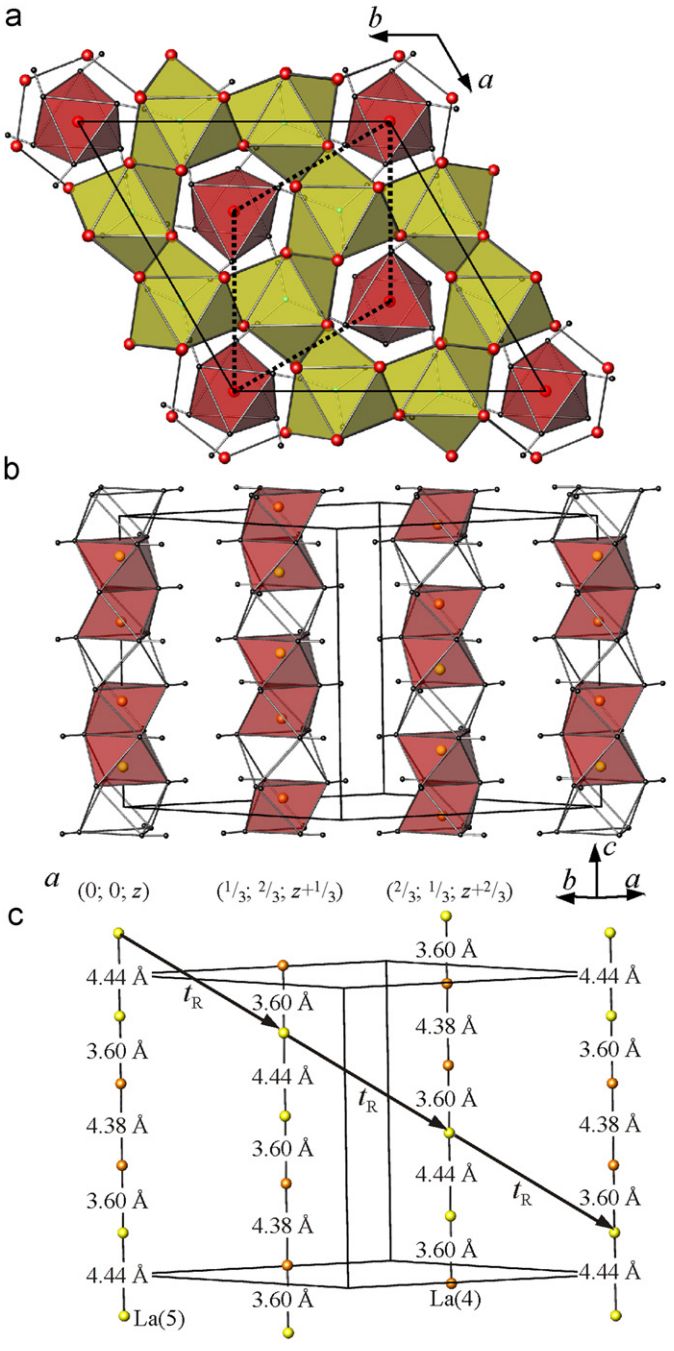

Fig. 2. (*a*) [0001] projection of the crystal structure of $La_{11}[MnC_6]_3$, emphasizing the network of MnC_6@La_9 polyhedra (yellow) with hexagonal channels accommodating La@C_6 octahedra (red); the $P6_3/m$ subcell is shown by dashed line, while the $R\bar{3}$ supercell ($a=\sqrt{3}a_0$; $c=3c_0$) is indicated by solid line. (*b*) Columns of face-sharing carbon octahedra filled by La atoms running along *c*-axis. (*c*) La chains with alternating La–La distances; translation corresponding to the *R*-cell, t_R, is shown by the arrow. (For interpretation of the references to color in this figure legend, the reader is referred to the web version of this article.)

3.2. $La_{11}(MnC_6)_3$

The carbides $RE_{3.67}TC_6$ (*RE*=La–Nd, Sm; *T*=Fe, Ru, Mn) were first reported by Witte and Jeitschko [4] to crystallize in the hexagonal space group $P6_3/m$ (No 176) with the unit cell parameters $a_0=8.806(1)$ Å and $c_0=5.329(1)$ Å for $La_{3.67}MnC_6$ and $a_0=8.787(2)$ Å and $c_0=5.351(1)$ Å for $La_{3.67}FeC_6$. In the crystal structure of $La_{3.67}FeC_6$ one of the lanthanum sites (Wyckoff site 4*e*, with coordinates (0, 0, *z*)) is occupied by $\frac{1}{3}$ only, which implies a significant degree of disorder within the lanthanum sublattice. The structure reported in this work is a new variant of superstructure of $La_{3.67}MnC_6$ ($R\bar{3}$ (*No* 148); $a=\sqrt{3}a_0$; $c=3c_0$) with a ninefold enlarged cell volume and complete ordering of the La atoms. La atoms occupy three 18*f* and two 6*c* positions, C atoms are located in six 18*f* positions, and there is only one 18*f* Mn site. All the positions are fully occupied, leading to the overall composition $La_{66}Mn_{18}C_{108}$ or $La_{11}(MnC_6)_3$ with *Z*=6.

The crystal structure of $La_{11}(MnC_6)_3$ features trigonal planar $Mn(C_2)_3$ units with three carbon atoms bonded to the manganese atoms at a distance of 1.82–1.83 Å and additional three terminal carbon atoms, which form homonuclear bonds only (Fig. 1). The C–C bond distance (1.32–1.36 Å) is closer to that of ethylene (1.34 Å [17]) than acetylene (1.20 Å [17]), indicating its double bond nature; however additional quantum chemical studies are necessary to clarify this issue. The $Mn(C_2)_3$ units show slight deviation from planarity with C–Mn–C angle of 118.9° instead of

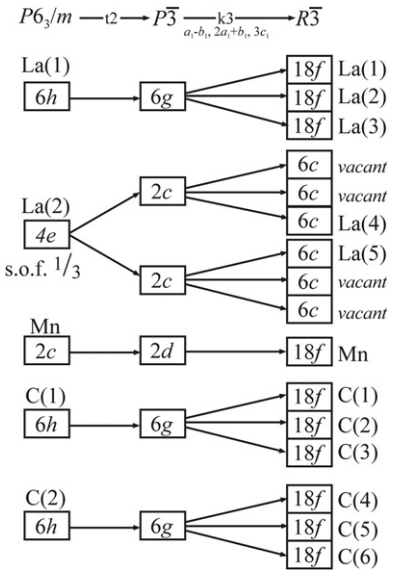

Scheme 1. Group–subgroup relationship for $La_{11}(MnC_6)_3$ using the formalism of ref. [19] and demonstrating the splitting of the Wyckoff positions during the transformation from the space group $P6_3/m$ to the space group $R\bar{3}$.

120°. Each of these MnC_6 complex anions is surrounded by nine La atoms forming a tricapped trigonal prism centered by the manganese atom. The MnC_6@La_9 prisms are connected with each other by sharing common trigonal faces and form infinite chains running along the *c*-axis. These chains are further linked via common faces in the *ab*-plane giving a rise to a three-dimensional framework with large hexagonal channels. Within the hexagonal channel the terminal carbon atoms of the $Mn(C_2)_3$ units form columns of face-sharing octahedra with long, essentially non-bonding C–C distances of 3.5–3.7 Å. The carbon octahedra accommodate the remaining lanthanum atoms located in La(4) and La(5) positions. These sites are situated in such a way that one empty carbon octahedron is followed by two filled ones; therefore only $\frac{2}{3}$ of the face-sharing carbon octahedra are centered by La atoms (Fig. 2). The La atoms are found not in the exact center of the carbon octahedra but rather shifted toward one of the trigonal faces in order to attain more favorable La–C distances of 2.60 Å (vs. hypothetical 2.81 Å for La in the center of the carbon octahedron). This arrangement of La atoms within the carbon octahedra leads to La-chains (La(4)–La(4)–La(5)–La(5)–La(4)) running along the *c*-axis, with alternating La–La distances of 4.38 – 3.60 – 4.44 – 3.60 Å. The neighboring chains are shifted with respect to each other by $t_R(\frac{1}{3},\frac{2}{3},\frac{1}{3})$, thus defining the *R*-centering.

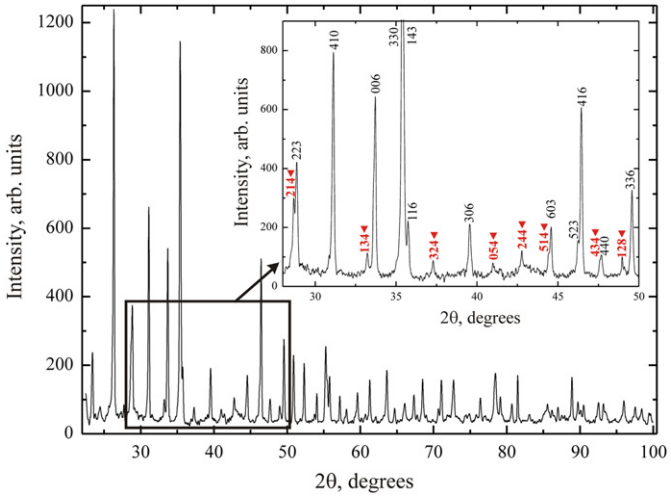

Fig. 3. The X-ray powder pattern of $La_{11}(MnC_6)_3$. Inset: section of the pattern in the range $28^\circ \le 2\theta \le 50^\circ$; the superstructure reflections are indicated by red arrows. (For interpretation of the references to color in this figure legend, the reader is referred to the web version of this article.)

The transformation from subcell ($P6_3/m$) to supercell ($R\bar{3}$; $a=\sqrt{3}a_0$; $c=3c_0$) in the case of $La_{11}(MnC_6)_3$ includes a ninefold cell volume increase and a change of the centering and symmetry. Since $R\bar{3}$ is not a maximal nonisomorphic subgroup of $P6_3/m$ according to the International Tables for Crystallography [18], the transformation from $P6_3/m$ to $R\bar{3}$ can be described as a combination of "klassengleich" (class-equivalent) and "translationengleich" (lattice-equivalent) symmetry reductions [19]. The corresponding relationship between $P6_3/m$ and $R\bar{3}$ space groups and the transformation of the Wyckoff positions [20] are shown in Scheme 1. Upon such transformation the lanthanum position 4*e* with the partial occupancy of $\frac{1}{3}$ in the subcell ($P6_3/m$) is split into six 6*f* positions ($R\bar{3}$). Only two of them are found to be occupied, thus resulting in complete ordering of La atoms. Examination of the X-ray powder pattern of a powdered sample of $La_{11}(MnC_6)_3$ (Fig. 3) revealed the presence of weak but noticeable reflections which contradict the subcell symmetry ($P6_3/m$; $a=a_0=8.8035$ Å; $c=c_0=5.3346$ Å), but could be indexed in the supercell proposed here ($R\bar{3}$; $a=\sqrt{3}a_0$; $c=3c_0$). This confirms the adoption of the superstructure in the bulk sample of $La_{11}(MnC_6)_3$.

Another superstructure variant was recently reported for the carbide $La_{3.67}FeC_6$. This type of superstructure is described by the tripling of the *c*-edge ($P6_3/m$; $a=a_0=8.7926(8)$ Å, $c=3c_0=16.046(1)$ Å)) [5]. While the overall structure motif is the same, the major difference between subcell and supercell derives from the positioning of La atoms within the column of face-shared carbon octahedra. In the subcell the La chain running along *c*-axis is described as one La position (0, 0, *z*) with the occupancy of $\frac{1}{3}$, while in the $P6_3/m$ supercell with the tripled *c*-edge there are two La positions (0, 0, z_1) and (0, 0, z_2). These positions have occupancies of $\frac{1}{2}$, since the resulting La–La distances in the case of full occupancy are unreasonably short. Thus occupational disorder in La positions is still present even in the $P6_3/m$ supercell with tripled *c*-edge. This

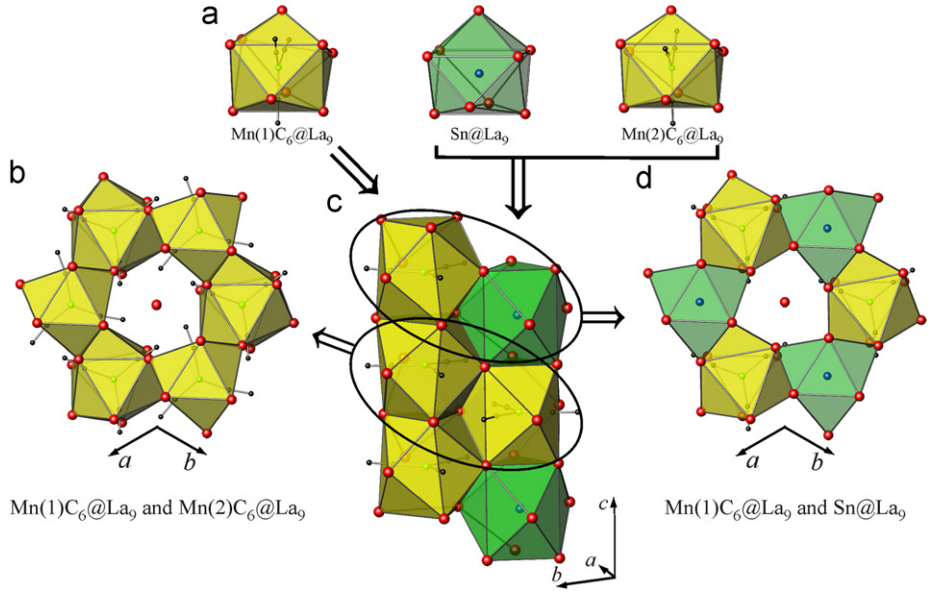

Fig. 4. Different fragments found in the crystal structure of $La_{14}Sn(MnC_6)_3$. (*a*) Tricapped trigonal prisms of La atoms centered by MnC_6 (yellow) or Sn (green). (*b*) and (*d*) Two types of [0001] layers formed by MnC_6@La_9 and Sn@La_9. (*c*) Two types of columns running along *c*-axis produced by $Mn(1)C_6$@La_9 only or by a combination of $Mn(2)C_6$@La_9 and Sn@La_9. (For interpretation of the references to color in this figure legend, the reader is referred to the web version of this article.)

description results in the superposition of two La chains with alternating La–La distances of 3.40 and 4.62 Å different in their relative shift along *c*-axis. A similar kind of superstructure with a tripled *c*-edge was reported for $La_{3.65}RuC_6$ [6] but this was refined as a commensurate modulated structure. Carbides $La_{3.67}FeC_6$ and $La_{3.65}RuC_6$ were prepared by a conventional method, e.g. arc-melting of the starting components followed by long-term annealing. The new and completely ordered $R\bar{3}$ superstructure variation reported here for $La_{11}(MnC_6)_3$ might stem from the different *d*-metal (manganese) and synthesis method (flux growth from La/Ni eutectic flux). No order–disorder phase transitions were observed in DSC experiments on $La_{11}(MnC_6)_3$. The possibility of annealing a disordered variant ($La_{3.67}MnC_6$) to promote formation of the $R\bar{3}$ superstructure cannot be excluded, although the energy difference between the superstructure and subcell may be very small due to the very subtle structural differences.

3.3. $La_{14}Sn(MnC_6)_3$

The crystal structure of quaternary carbide $La_{14}Sn(MnC_6)_3$ (Fig. 4) is closely related to that of $La_{11}(MnC_6)_3$. Similar $Mn(C_2)_3$ groups (Fig. 1a) are found in the center of tricapped trigonal prisms of La atoms (Fig. 4). There are two manganese atom positions, Mn(1) and Mn(2), with similar trigonal-planar coordination by three C_2 units; slight deviation from the planarity of the MnC_6-unit is observed for Mn(1) (C–Mn–C angle 119.86(2)°), while $Mn(2)C_6$ is perfectly planar. The manganese atoms are further coordinated by nine La atoms, forming tricapped trigonal prisms; $Mn(1)C_6@La_9$ is more distorted than $Mn(2)C_6@La_9$ (Fig. 4). The nine-vertex coordination polyhedron around the tin atoms, $Sn@La_9$, has a similar shape as that for $MnC_6@La_9$ (Fig. 4) and the La–Sn distances of 3.42 – 3.56 Å are comparable to the La-Mn distances of 3.23 – 3.64 Å. Thus Sn atoms can "mimic" MnC_6-units in their coordination by lanthanum atoms; $La_{11}(MnC_6)_3$ and $La_{14}Sn(MnC_6)_3$ can be viewed as being comprised of very similar building blocks. The $Sn@La_9$ polyhedron is a commonly observed building block in other La-rich phases obtained from La/Ni eutectic flux. This moiety might form in the molten flux during synthesis and act as a template for the final product, adopting slightly different shapes depending on the crystallizing phase. For the cubic phase $La_{21}T_8E_7C_{12}$ [8,16] (T=Fe, Mn; E=Ge, Sn, Sb, Te, Bi) the $Sn@La_9$ polyhedron has a shape of a monocapped square antiprism, while in the structure of $La_6SnNi_{3.67}Ru_{0.76}Al_{3.6}$ [9b] the tin atom is coordinated by nine La atoms forming a tricapped trigonal prism. Synthesis in La/Ni eutectic flux in the presence of heavy main elements other than Sn (e.g. M=Ge, Sb, Te, Bi) does not lead to the quaternary carbide phase $La_{14}M(MnC_6)_3$, suggesting that the $Sn@La_9$ cluster might be one of the most stable specimens in the La/Ni eutectic melt.

The Sn- or MnC_6-centered polyhedra of La atoms are linked by sharing common trigonal faces to form columns of two different types running along the *c*-axis (Fig. 4). The first type of column is formed by distorted $Mn(1)C_6@La_9$ polyhedra only, while the second type of column is built of alternating $Mn(2)C_6@La_9$ and $Sn@La_9$ units. In the *ab*-plane these polyhedra share common faces to form two different kinds of layers comprised of La polyhedra either with MnC_6 units only or $Mn(1)C_6$ and Sn (Fig. 4). As is also seen for the ternary carbide $La_{11}(MnC_6)_3$, the terminal carbon atoms of $Mn(C_2)_3$ units form columns of face-sharing carbon octahedra with long C–C distances of 3.40–3.60 Å. The chain of carbon octahedra runs along the *c*-axis inside the hexagonal channel defined by $X@La_9$ units (X=MnC_6 or Sn). La(4) atoms fill the carbon octahedra with a La–La distance of 3.58 Å. The carbon octahedra do not form a continuous column along the *c*-axis as is seen in the structure of $La_{11}(MnC_6)_3$; instead, these octahedra are coupled in pairs with an empty space between them, corresponding to a missing block of two octahedra (Fig. 5). The missing block is a result of incorporation of tin into the structure instead of MnC_6 units, since the empty space between pairs of carbon octahedra is surrounded by $Sn@La_9$ polyhedra. One of the lanthanum sites of the $Sn@La_9$ polyhedron is split into two positions, La(3) and La(3a), with a 0.89/0.11 ratio. La(3a) is shifted in the *ab*-plane toward the center of the empty void where the carbon octahedron is missing.

Taking the structural similarities into account, the composition of quaternary phase $La_{14}Sn(MnC_6)_3$ can be directly derived from that of ternary $La_{11}(MnC_6)_3$ as shown in Scheme 2. The composition of $La_{3.67}MnC_6$ (e.g. composition $La_{11}(MnC_6)_3$ divided by 3) can be represented as $La_{12}La_{2.67}Mn_4C_{24}$ by multiplying the formula by

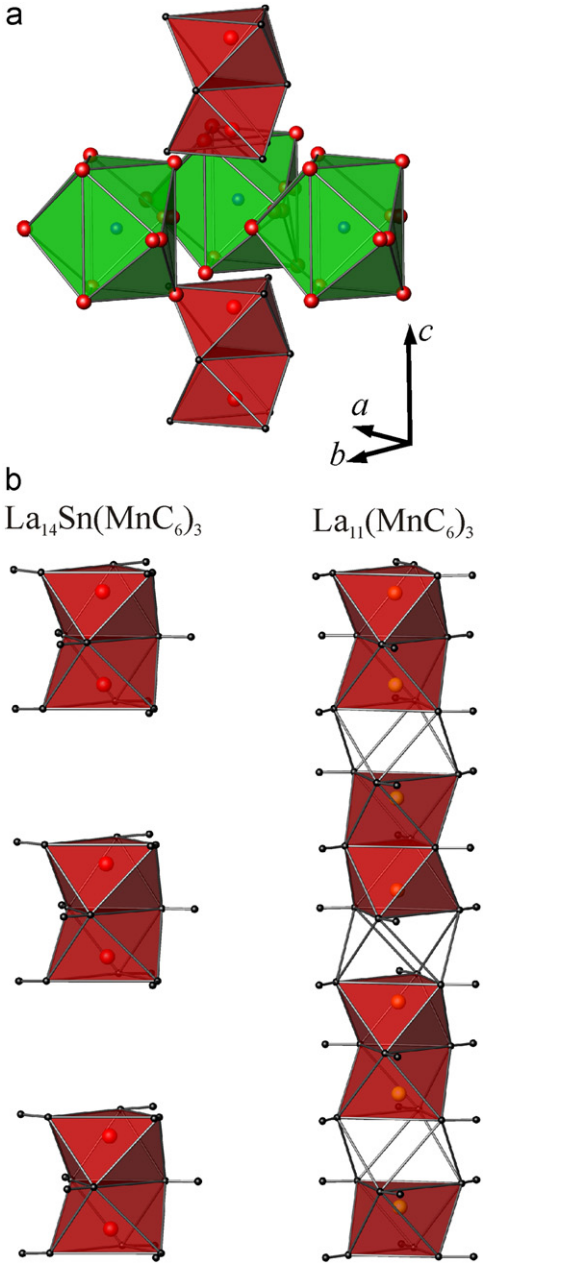

Fig. 5. (*a*) Fragment of the crystal structure of $La_{14}Sn(MnC_6)_3$ showing the pairs of carbon octahedra (red) filled by La atoms and surrounding $Sn@La_9$ polyhedra (green); (*b*) the columns of face-sharing carbon octahedra $La@C_6$ found in the crystal structure of $La_{14}Sn(MnC_6)_3$ and of $La_{11}(MnC_6)_3$; note the different periodicity of carbon octahedra filling by La atoms. (For interpretation of the references to color in this figure legend, the reader is referred to the web version of this article.)

four and distinguishing the 12 La atoms which form polyhedra around Mn atoms from the La atoms which occupy the columns of face-sharing carbon octahedra. Within such columns, two octahedra filled by La atoms are followed by one empty octahedron, thus "$La_{2.67}$" corresponds to "$(La_4)_{2/3}$". In the quaternary phase one of the MnC_6@La_9 units is replaced by a Sn@La_9 unit. Moreover, the filling of the column of face-sharing carbon octahedra by La atoms differs for $La_{11}(MnC_6)_3$ and $La_{14}Sn(MnC_6)_3$. Instead of the FF*E*FF*E* sequence (F-filled octahedron, *E*- empty octahedron) as is seen in the ternary phase, the FF*EE*FF*EE* sequence is observed in the quaternary phase; thus only $\frac{1}{2}$ of these carbon octahedra are filled. So instead of "$(La)_{\frac{2}{3}}$" the number of La atoms within the chain for the tin-containing phase could be expressed as "$(La)_{\frac{1}{2}}$", hence resulting in experimentally observed composition $La_{12}La_2SnMn_3C_{18}$ or concisely $La_{14}SnMn_3C_{18}$.

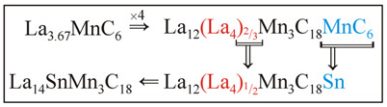

Scheme 2. The compositional relationship between $La_{11}(MnC_6)_3$ and $La_{14}SnMn_3C_{18}$. For the matter of clarity $La_{11}(MnC_6)_3$ is denoted as "$La_{3.67}MnC_6$".

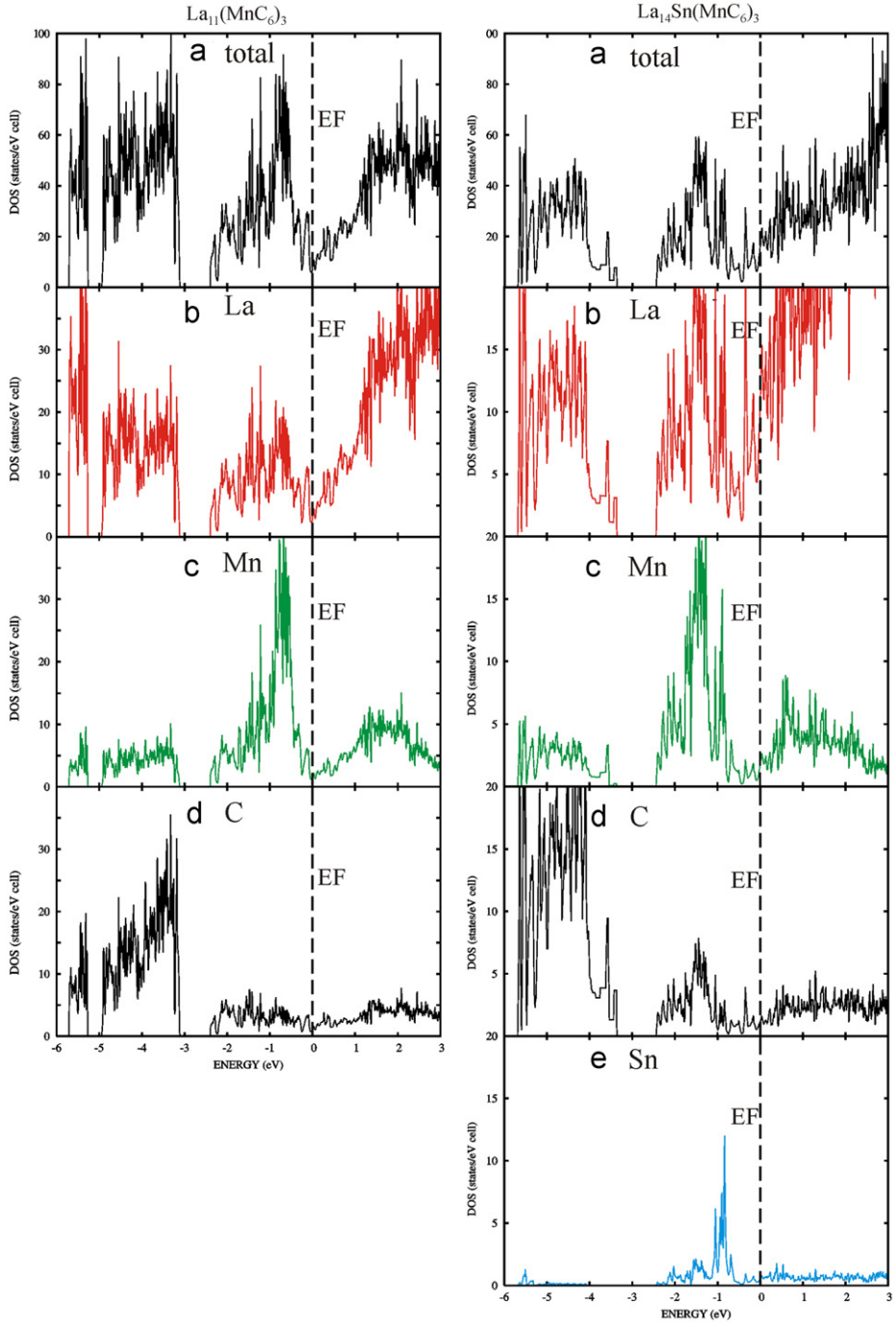

Fig. 6. (*a*) Total density of states (DOS) for $La_{11}(MnC_6)_3$ (left) and $La_{14}Sn(MnC_6)_3$ (right). The partial DOS for (*b*) La; (*c*) Mn; (*d*) C; (e) Sn are color-coded.

3.4. Electronic structure

The density of states (DOS) diagram for ternary $La_{11}(MnC_6)_3$ and quaternary $La_{14}Sn(MnC_6)_3$ carbide phases are similar. The Fermi level falls in a pseudogap in the DOS for both, with the small but non-zero DOS at E_F indicating metallic behavior (Fig. 6). The deeply lying states between -9 and -6 eV originate from carbon and tin (for $La_{14}Sn(MnC_6)_3$) *s*-states, manganese *s*- and *d*-states and lanthanum *d*-states. The states in the valence region between -6 eV and the Fermi level are mainly composed of C-2*p*, Sn-5*p*, La-5*d*, and Mn-3*d* states. Lanthanum *d*-states make the largest contribution to the states at the Fermi level.

The effect of lanthanum atom ordering on the electronic properties of $La_{11}(MnC_6)_3$ is highlighted by comparing the data in Fig. 6 to data for a similar compound. A detailed analysis of electronic structure and chemical bonding was recently reported for the Ru-carbide $La_{3.65}RuC_6$ [6]. The structure model used for this calculation corresponds to the threefold superstructure ($P6_3/m$; $a=a_0$, $c=3c_0$) with imposed averaged distances between the La atoms inside the chain of carbon octahedra. The overall DOS for $La_{3.65}RuC_6$ is similar to that of $La_{11}(MnC_6)_3$, with La–La interactions dominating at the Fermi level, E_F. However, in the disordered Ru analog, the La states produce a substantial DOS peak at E_F (estimated from [6]: $N_{La}(E_F)=5$ states/eV per $La_{3.65}RuC_6$ formula unit) whereas the ordered Mn analog studied here features a pseudogap at the Fermi level ($N_{La}(E_F)=0.5$ states/eV per $La_{3.67}MnC_6$ formula unit). The ordering of La atoms with optimized La–La distances probably leads to the stabilization of the crystal structure as can be concluded from the removal of the large DOS peak at E_F (which is indicative of instability).

4. Conclusion

Crystal growth from the La/Ni eutectic flux was used to synthesize ternary $La_{11}(MnC_6)_3$ and new quaternary $La_{14}Sn(MnC_6)_3$ carbide phases. The crystal structures of both phases have similar structural fragments, i.e. trigonal planar $Mn(C_2)_3$ units surrounded by nine La atoms. $La_{11}(MnC_6)_3$ features a new type of superstructure with complete ordering of La atoms within the column of face-sharing carbon octahedra. The replacement of some of the $Mn(C_2)_3$ units with Sn atoms in the case of $La_{14}Sn(MnC_6)_3$ breaks the continuous column into pairs of carbon octahedra filled with La atoms. Calculation of electronic structure indicates that arrangement of La atoms has crucial impact on the stability of discussed carbides. Isolation of the $La_{14}Sn(MnC_6)_3$ phase is another indication of the stability of the $Sn@La_9$ building block in La/Ni flux. Additional exploration of this flux and related fluxes such as Ce/Ni or Ce/Co, which are also suitable for the crystallization of new carbide phases, is proving to be of great interest and these studies are in progress.

Acknowledgments

This research made use of the Scanning Electron Microscope facilities of MARTECH at Florida State University. Financial support from the NSF (Grant DMR-05-47791) is gratefully acknowledged.

Appendix A. Supplementary materials

Supplementary data associated with this article can be found in the online version at doi:10.1016/j.jssc.2010.10.004.

References

[1] (a) W. Scherer, C. Hauf, M. Presnitz, E.W. Scheidt, G. Eickerling, V. Eyert, R.D. Hoffmann, U.C. Rodewald, A. Hammerschmidt, C. Vogt, R. Pöttgen, Angew. Chem. Int. Ed. 49 (2010) 1578–1582;
(b) V.K. Pecharsky, L.L. Miller, K.A. Gschneidner Jr., Phys. Rev. B 58 (1998) 497–502;
(c) M.H. Gerdes, W. Jeitschko, K.H. Wachtmann, M.E. Danebrock, J. Mater. Chem. 7 (1997) 2427–2431.
[2] (a) X.D. Wen, T.J. Cahill, N.M. Gerovac, M.J. Bucknum, R. Hoffmann, Inorg. Chem. 49 (2010) 249–260;
(b) B. Rohrmoser, G. Eickerling, M. Presnitz, W. Scherer, V. Eyert, R.D. Hoffmann, U.C. Rodewald, C. Vogt, R. Pöttgen, J. Am. Chem. Soc. 129 (2007) 9356–9365;
(c) E. Dashjav, Y. Prots, G. Kreiner, W. Schnelle, F.R. Wagner, R. Kniep, J. Solid State Chem. 181 (2008) 3121–3130.
[3] E. Dashjav, G. Kreiner, W. Schnelle, F.R. Wagner, R. Kniep, W. Jeitschko, J. Solid State Chem. 180 (2007) 636–653.
[4] A.M. Witte, W. Jeitschko, Z. Naturforsch. B51 (1996) 249–256.
[5] B. Davaasuren, E. Dashjav, G. Kreiner, H. Borrmann, R. Kniep, J. Solid State Chem. 182 (2009) 1331–1335.
[6] B. Davaasuren, E. Dashjav, T. Doert, G. Kreiner, W. Schnelle, F.R. Wagner, M. Mihalkovič, R. Kniep, Z. Anorg. Allg. Chem. 636 (2010) 41–49.
[7] M.G. Kanatzidis, R. Pöttgen, W. Jeitschko, Angew. Chem. Int. Ed. 44 (2005) 6996–7023.
[8] E.M. Benbow, N.S. Dalal, S.E. Latturner, J. Am. Chem. Soc. 131 (2009) 3349–3354.
[9] (a) E.M. Benbow, N.S. Dalal, S.E. Latturner, J. Solid State Chem. 182 (2009) 3055–3062;
(b) J.V. Zaikina, Y.J. Jo, S.E. Latturner, Inorg. Chem. 49 (2010) 2773–2781.
[10] SAINT; Bruker AXS Inc.: Madison, WI, 2008.
[11] SADABS; Bruker AXS Inc.: Madison, WI, 2008.
[12] G.M. Sheldrick, Acta Crystallogr. A64 (2008) 112–122.
[13] A.L. Spek, J. Appl. Cryst. 36 (2003) 7–13.
[14] L.G. Akselrud, P.Y. Zavalij, Y. Grin, V.K. Pecharsky, B. Baumgartner, E. Wölfel, Mater. Sci. Forum 133-136 (1993) 335–351.
[15] (a) O. Jepsen, A. Burkhardt, O.K. Andersen, The Program TB-LMTO-ASA, version 4.7 (2000), Max-Planck-Institut für Festkörperforschung: Stuttgart, Germany;
(b) P.E. Blöchl, O. Jepsen, O.K. Andersen, Phys. Rev. B: Condens. Matter Mater. Phys. 49 (1994) 16223–16233.
[16] J.V. Zaikina, I. Schellenberg, E.M. Benbow, R. Pöttgen, S.E. Latturner, Chem. Mater. (submitted 2010).
[17] M.A. Fox, J.K. Whitesell, Organische Chemie—grundlagen, mechanismen, bioorganische Anwendungen, Spektrum Akademischer Verlag, Heidelberg, 1995.
[18] International Tables for Crystallography, Vol. A, (Ed.: T. Hahn), Kluwer, Dordrecht, 1989, chapter 7, p. 672.
[19] H. Bärnighausen, MATCH 9 (1980) 139–175.
[20] (a) E. Kroumova, J.M. Perez-Mato, M.I. Aroyo, J. Appl. Cryst. 31 (1998) 646;
(b) S. Ivantchev, E. Kroumova, M.I. Aroyo, J.M. Perez-Mato, J.M. Igartua, G. Madariaga, H. Wondratschek, J. Appl. Cryst. 35 (2002) 511–512.